JOURNAL OF MATERIALS SCIENCE **35** (2000) 2263–2271

The effect of supercooling on the microstructure of Al-Nb alloys

A. MUNITZ
Nuclear Research Center-Negev, P.O. Box 9001 Beer-Sheva, Israel

A. B. GOKHALE
Dayton T. Brown, Inc., Bohemia, NY 11716, USA

R. ABBASCHIAN
University of Florida, Gainesville, Florida 32611, USA

Electromagnetic levitation was used to study supercooling effects on solidification characteristics of Al-Nb alloys containing 15–53 at.% Nb. The results indicate that Al_3Nb, with a melting temperature of 1980 K, is not a stoichiometric line compound but has a homogeneity range on the Nb side. These results are consistent with the more recently assessed Al-Nb phase diagram, but not with those assessed previously. Significant changes in the microstructural morphology of Al-40 at.% Nb were also observed as a function of the bulk supercooling. These include metastable compositional extensions of Al_3Nb, preferential nucleation of Al_3Nb in the supercooled liquid and corresponding changes in the solidification path. For example, spherical domains comprising of a mixture of Al_3Nb and $AlNb_2$ were revealed in the eutectic microstructure, their volume fraction being an increasing function of the degree of supercooling. Moreover, the Al_3Nb and $AlNb_2$ exhibited metastable compositional extensions up to 31 at.% for the former and down to 48 at.% Nb for the latter.

1. Introduction

Niobium base alloys are prime candidates for many high-temperature aerospace applications, by virtue of their high melting temperature, and excellent high-temperature creep resistance [1, 2]. These desirable properties have however been offset by poor ambient temperature ductility, fabricability, embrittlement after welding, and generally poor oxidation resistance above 923 K [1]. The increase in embrittlement, which is caused by diffusion of oxygen and nitrogen into the alloys, may be reduced if the alloys are protected by proper surface coatings. While alumindes, silicides and Ni-Cr alloys can be used as protective coatings, interdiffusion between the active coating and the substrate element limits the coating lifetime. In addition, surface coatings are frequently subject to failure by spalling or cracking by either thermal fatigue or impact. It has been shown [3] that using minor alloying additions, it may be possible to develop a niobium base alloy which forms a self protective coating in an oxidizing environment. Among the two most widely studied alloying elements, Al and Si are preferred due to the high stability of their oxides and slow oxygen diffusion through the oxide layers. The addition of Al or Si, however, causes the formation of brittle intermetallic compounds during conventional solidification [4]. It is anticipated that the high-temperature mechanical properties of such structural alloys may be altered and perhaps improved by rapid solidification processing (RSP) under bulk supercooling conditions. The processing may be utilized not only to obtain finer scale and more homogeneous microstructures, but also to change the solidification path and curb the formation of brittle phases.

The purpose of this work was to investigate the solidification microstructures of Al-Nb alloys containing between 15 and 53 at.% Nb under different conditions of bulk supercooling using an electromagnetic (EM) levitation techniques.

2. Experimental procedure

Niobium and aluminum (99.99% pure) samples, weighing approximately 1.5 grams, were alloyed by arc melting in an Ar environment using a non-consumable tungsten electrode. For each arc melted sample, the individual alloy components were weighed, with an accuracy of ± 0.01 grams, according to the desired bulk composition. The arc-melting period was kept relatively brief, normally a few seconds, to allow for the melting of Al and forming of a single button. Each arc melted button was then levitated and processed using an electromagnetic (EM) levitation apparatus described elsewhere [5–8]. During EM levitation, a typical sample processing cycle consisted of melting, superheating by about 100 to 200 K followed by cooling. Heating or cooling of the sample during levitation is accomplished by changing the rate of He/Ar gas mixture and/or changing the gas flow rate. Heating and cooling of the sample

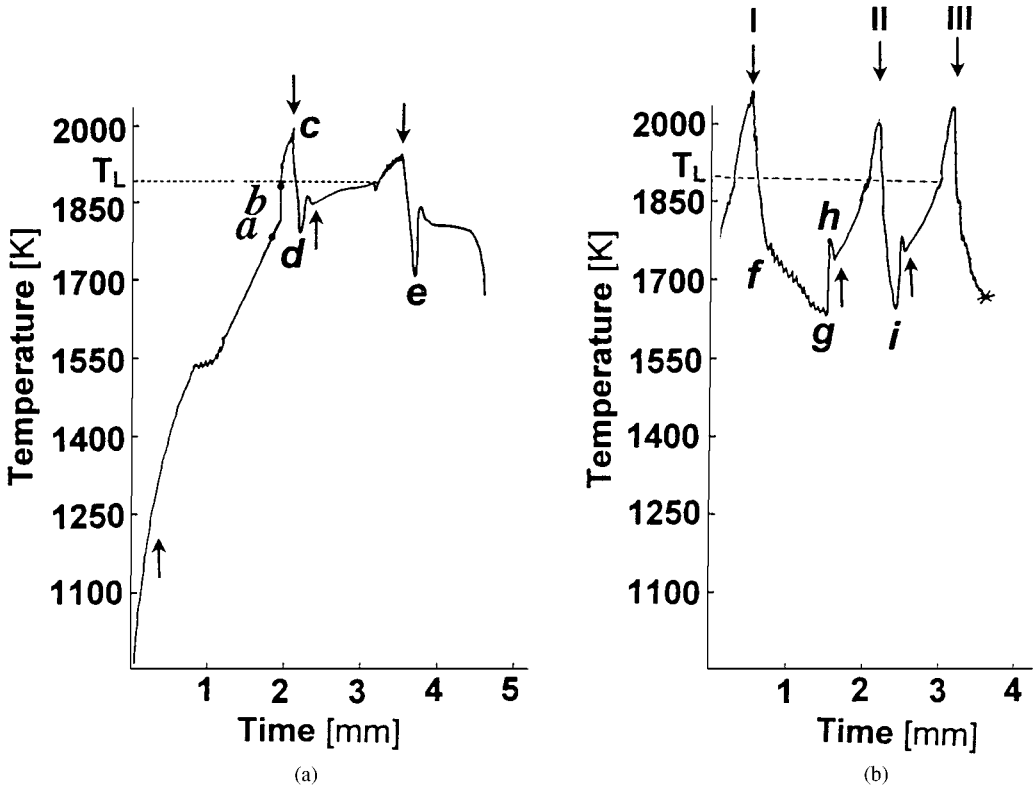

Figure 1 A typical thermal history of average sample temperature vs time for an Al 15 at.% Nb (a), and for 45 at.% Nb (b). The arrows indicate where the gas flow was adjusted to cause heating (↑) or cooling (↓) of the sample.

is indicated by the upward and downward arrows in the Fig. 1a, respectively. For a given alloy, the samples were released from various desired temperatures, e.g. from a superheated state, from the "solid + liquid" state, or from various degrees of supercooling, and quenched on a copper chill. Usually a few cycles of heating and cooling were performed before final quenching from the desired level of supercooling. The sample temperature was monitored continuously by a two-color optical pyrometer, connected to a strip chart-recorder. Supercoolings as high as 375 K were obtained.

After processing, the samples were cross-sectioned and prepared for analysis using standard metallographic procedures. Specimens with less than 40 at.% Nb were etched in a solution of 10 cc HF + 30 cc HNO_3 + 60 cc lactic acid, whereas specimens with higher Nb content were etched with a solution containing 5 cc HF + 20 cc HNO_3 + 50 cc CH_3COOH. The etching process continued for about 15 to 30 second until the microstructure was revealed. The microstructural and compositional analysis were carried out using optical microscopy, and scanning electron microscopy equipped with energy dispersive spectroscopy-EDS. For the EDS analysis, the specimens were etched very lightly, just sufficient to reveal the microstructure yet keep the surface roughness to a minimum. The raw intensity data were corrected with a standard ZAF computer program [9]. The accuracy of the EDS was ascertained by comparing the results for a random number of samples with those measured using wavelength dispersive spectroscopy (WDS) technique. For the latter, pure Nb and Al were used as standards. Under no instance, the difference between the two measurements were more than 0.3 at.%. Structural analyses were performed on some of the samples after mechanical polishing, using a Cu K_α tube at the following conditions: Voltage—40 kV; Current—40 mAmp; Scanning step of 0.02°/s.

3. Results

The initial thermal response during levitation melting of the arc melted alloys were indicative of the mixing of the two components, as well as reactive formation of phases. This is illustrated in Fig. 1 by the thermal histories of Al-15 at.% Nb and Al-45 at.% Nb alloys presented in Fig. 1a and b, respectively. Fig. 1a shows the first heating cycle of an aluminum-rich (15 at.% Nb) arc melted sample. A thermal arrest near 1550 K is observed during the first heating cycle and otherwise monotonic heating of the sample up to 1815 K. At this temperature a sharp exotherm exists (accompanied by a sudden increase in the sample brightness) and the sample temperature changes rapidly to 1925 K. The temperature continues to increase up to about 1980 K, where the gas flow is adjusted to cause cooling. The sharp exotherm was observed only during the first heating cycle; from the second cycle onwards one could observe only a thermal arrest at about 1893 K, beyond which the sample was fully liquid. In order to improve the understanding of the melting and solidification processes taking place in the Al 15 at.% Nb alloy, samples were quenched from several points, as marked by letters on the thermal history in Fig. 1a. The sample marked (a) was quenched from 1733 K (i.e. just before the onset of the exotherm). The specimen dropped immediately

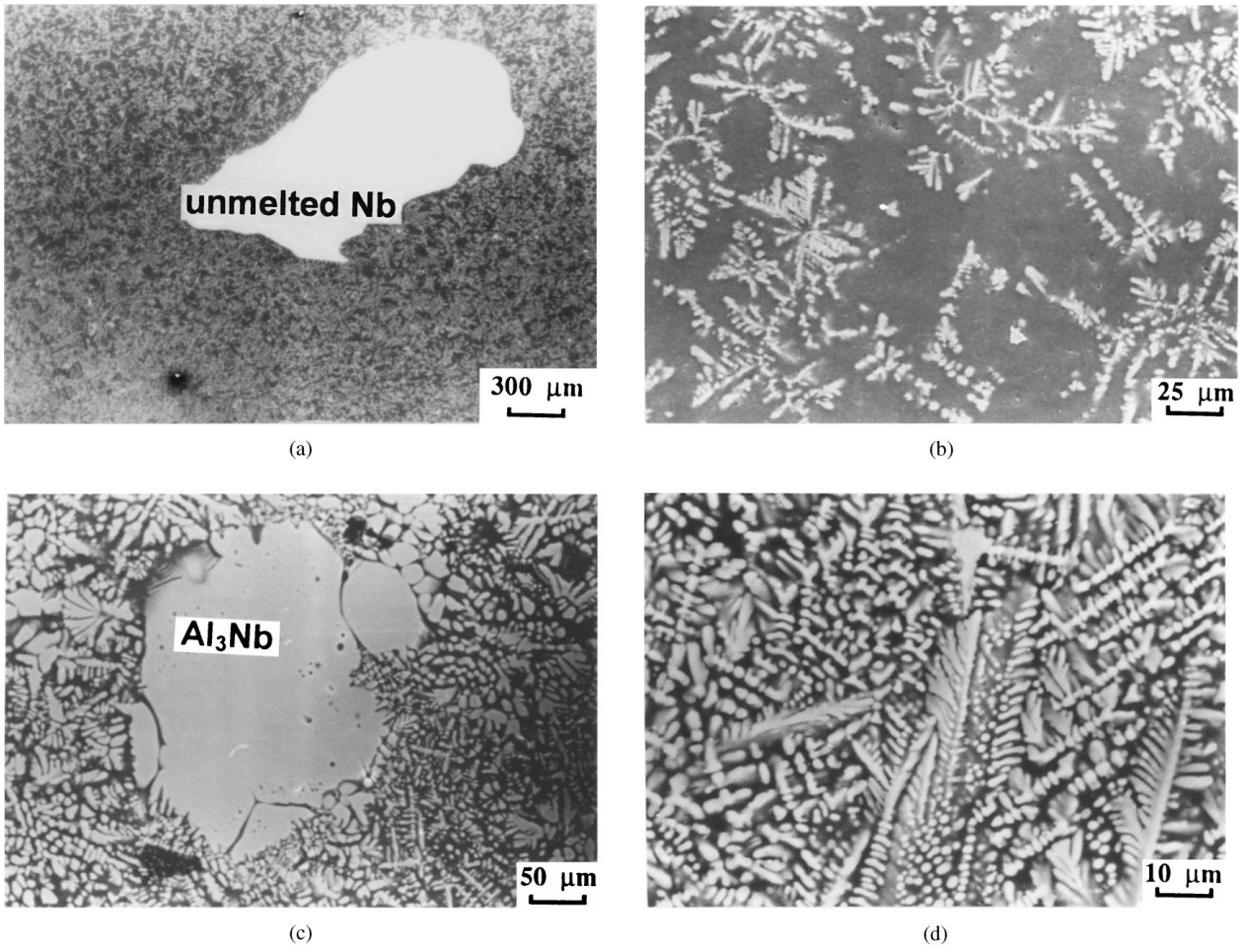

Figure 2 Secondary electron images illustrating the microstructure of Al 15 at.% Nb dropped from different temperatures as marked by letters in Fig. 1 for the first heating cycle. a, b) Sample dropped from 1733 K. c) dropped just after the sharp temperature increase, and d) quenched from above 1983 K.

following the exotherm is marked (b). The microstructure of these samples will be presented later in Fig. 2.

Upon cooling of the superheated liquid thermal arrests were observed which were indicative of nucleation and growth of various phases. This is shown in Fig. 1b for cooling of a superheated Al-45 at.% Nb liquid. A phase nucleates around point (f) in Fig. 1b, during the first cooling cycle as evidenced by the reduction in the temperature because of the release of the heat of solidification. Following this nucleation, the remaining liquid continues to supercool until a supercooling of 280 K point (g), where a second nucleation event takes place, accompanied by a massive recalescence to point (h). As discussed elsewhere [10, 11], while the first nucleation is followed by a slow growth, the second nucleation event is associated with the formation of a fast growing phase. Upon subsequent heating and cooling, cycle II, clearly only one major nucleation and growth is observed at point (h). The point designated by (*), in the last cycle denotes the temperature at which the fully liquid sample was released from the levitated state. The thermal arrests, indicated by T_L on the figure, represent the liquidus temperature of the alloy. In Figs 2 to 6, we present a series of secondary electron images (SEl's) illustrating the microstructure of various samples. Fig. 2a and b illustrate the microstructure of samples quenched from 1773 K (point a in Fig. 1a). In this sample, some undissolved Nb particles can be seen. It was found that each Nb particle was surrounded by a thin layer of an intermetalic phase, while the remaining matrix consisted of fine dendrites embedded in an aluminum matrix (Fig. 2b). Energy dispersive spectroscopy-EDS analysis indicated that the dendrites are Al_3Nb. The microstructure of Al 15 at.% Nb alloys quenched following the sharp exotherm (point b in Fig. 1a) is illustrated in Fig. 2c. The morphological similarity between the big particles apparent in both cases (compare Fig. 2a and c) indicates that they might originate from the same source, i.e., the unmelted pieces of Nb present in the arc-cast samples. The large particles in Fig. 2c, however, contain between 24 and 25 at.% Nb, i.e. they are Al_3Nb. As before, the rest of the sample contained fine Al_3Nb dendrites embedded in Al matrix. The Al_3Nb pieces similar to that shown in Fig. 2c, were observed in this and other samples as long as the quenching temperatures were below 1973 K after the first cycle. For the samples quenched from temperatures above 1983 K (Fig. 2d) no residual Al_3Nb particles was observed. This indicates that the melting temperature of Al_3Nb is close to 1983 K.

The microstructures of Al-15 at.% Nb samples solidified under different conditions are illustrated in Fig. 3a to d. Fig. 3a shows the microstructure of sample

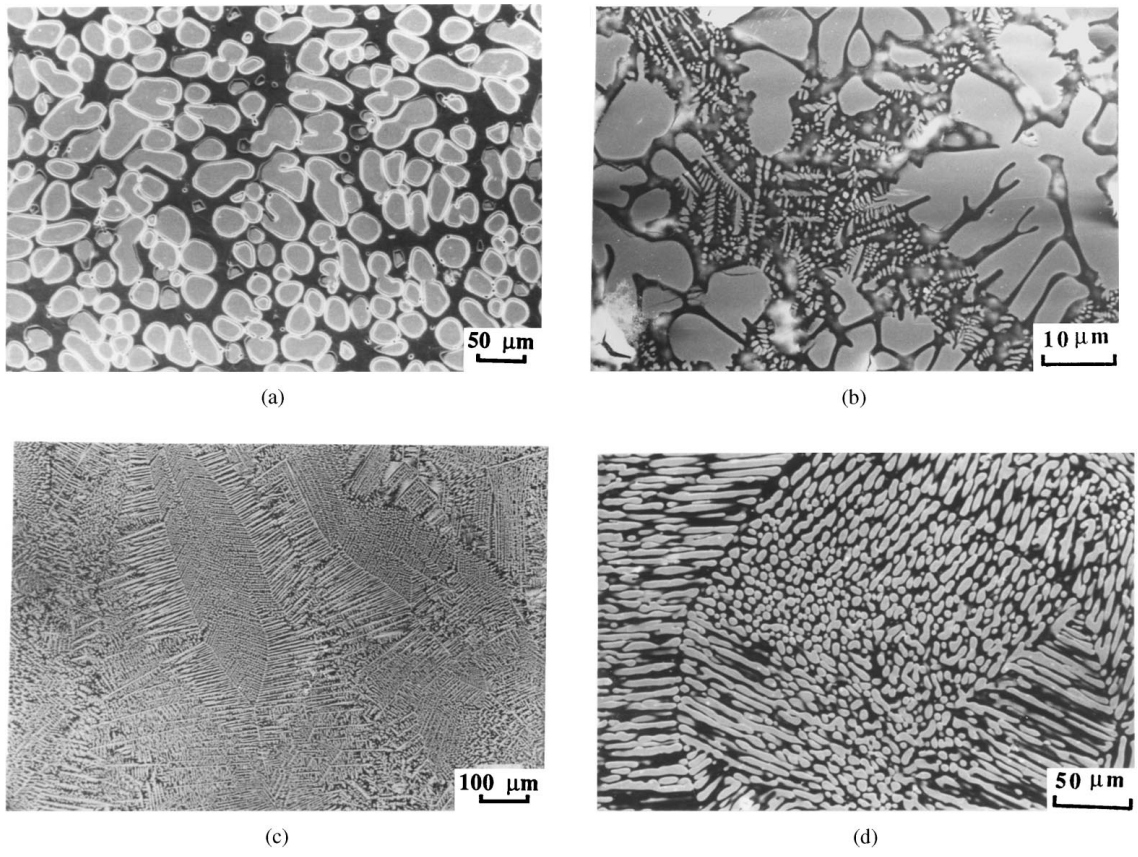

Figure 3 Secondary electron images illustrating the microstructure of Al 15 at.% Nb dropped after different supercooling conditions. a) solidified during levitation. b) quenched from the "liquid + solid" state. c) 100 K supercooling. d) 375 K supercooling.

quenched after solidification in the levitated state with negligible bulk supercooling. The microstructure consists of coarse Al_3Nb semi-spherical particles embedded in an Al matrix (gray phase in the figure). The Al_3Nb phase contained as high as 26.5 at.% Nb. Samples which where quenched from the "solid + liquid" state, Fig. 3b, contained coarse and fine Al_3Nb. The latter emerged from the former ones, indicating that the coarse dendrites grew during solidification in the levitation apparatus (low cooling rates) while the finer ones solidified under the high cooling rates against the Cu chill.

In general, the shape and thickness of the samples quenched against the copper chill depended on the temperature and state of sample (liquid or liquid + solid) prior quenching. The splats from fully liquid state were pancake shaped with somewhat thicker edges than the center, which was around 1 mm. The splats from the solid + liquid samples were generally much thicker and semi-spherical in shape. The sample quenched from the solid state had a pear shape.

The microstructure of the alloy supercooled by 100, and 375 K before quenching are shown in Fig. 3c to d, respectively. In each case, the morphology showed well-defined dendrite colonies. The boundary between dendrite colonies, consisting predominantly of the primary phase, can be seen in Fig. 3c. The specimen with high supercooling had finer microstructures, as illustrated in Fig. 3d. Note that these microstructures were obtained at locations approximately 500 μm away from the chill surface.

The microstructures of the Al-40 at.% Nb alloys are presented in Figs 4 to 5. The samples quenched from the liquid (superheated) and "liquid + solid" state are illustrated in Fig. 4a and b, respectively. In general, the microstructure in the thicker zone of the splats consisted of very long primary Al_3Nb dendrites containing 25 to 26.5 at.% Nb, embedded in a eutectic matrix. As before, the microstructure of samples quenched from the "solid + liquid" state (Fig. 4b) was coarser than the samples quenched from the superheated liquid. Structural analysis performed on samples which solidified during EM levitation, as well as samples solidified under different supercooling levels reveal the existence of only Al_3Nb and $AlNb_2$ phases.

Supercooling of Al-40 at.% Nb caused significant morphological change in the microstructure, as shown in Fig. 4c–f. Instead of the Al_3Nb dendrites, two-phase spherical domains were observed. Within each domain columnar Al_3Nb cells were seen radiating out towards the domain boundary where they were surrounded by a eutectic matrix. The details of the spherical domain/eutectic boundary with radiating columnar Al_3Nb are shown in Fig. 4e and f. It can be seen that the domain interior is indeed highly equiaxed. Within the domains themselves, the microstructure consists of primary Al_3Nb surrounded by a gray phase, which was embedded in a eutectic matrix. The Al_3Nb exhibits faceting tendency, and in some instances forms columnar dendrites, while the eutectic is of regular lamellar appearance. The volume fraction of the spherical domains increased with the supercooling, and

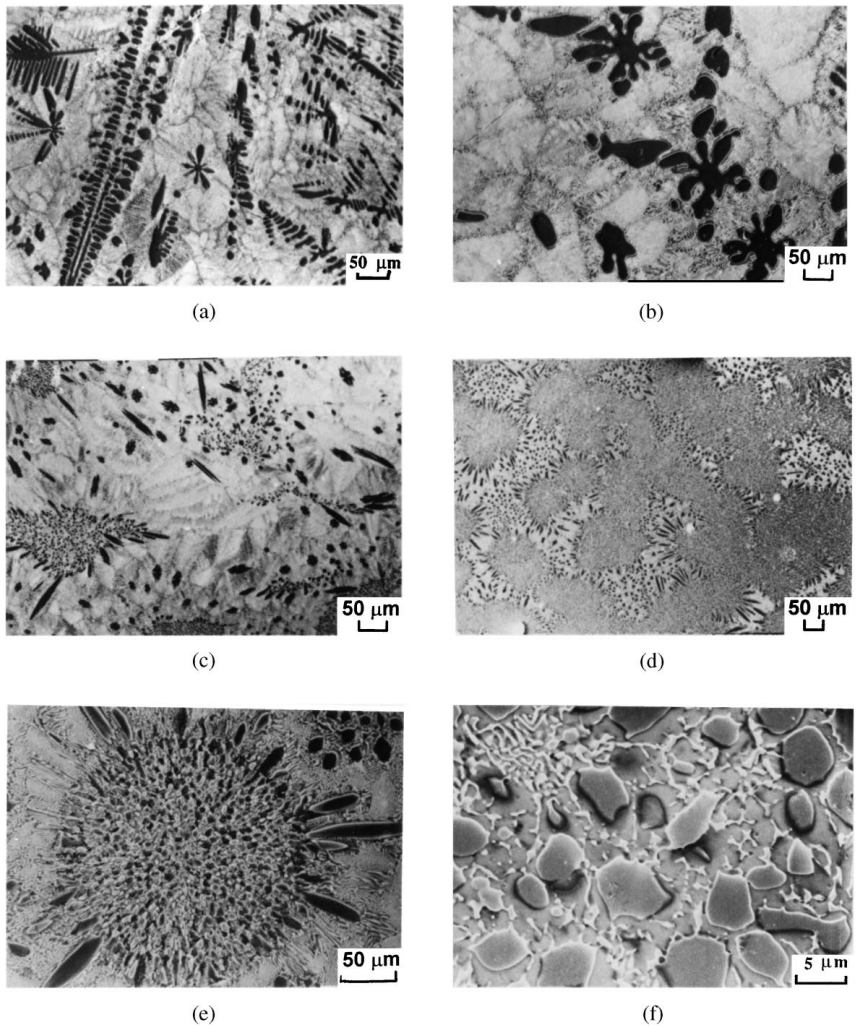

Figure 4 Secondary electron images illustrating the microstructure of Al 40 at.% Nb dropped after different conditions: a) from the "liquid" state. b) from the "liquid + solid" state. c) from 80 K supercooling. d) from 230 K supercooling. e) spherical domains with columnar Al_3Nb radiating out at the boundaries in alloy dropped after supercooling of 150 K. f) central region of the spherical domain in an alloy dropped from 240 K supercooling.

exceeded that of the eutectic matrix above 150 K. The primary Al_3Nb in the domains contain between 26 and 31 at.% Nb, while the gray phase surrounding it contained at least 48 at.% Nb (the Nb content of the matrix surrounding the particles may be underestimated due to its small dimensions).

A unique microstructure was observed in some Al-40 at.% Nb specimens which were dropped with small superheating on the copper chill, as presented in Fig. 5a to b. This microstructure was frequently observed in the thinner sections of the samples, and consisted of Al_3Nb crosses embedded in a regular eutectic microstructure. Microprobe microanalysis indicated that these crosses contain between 26 and 28 wt.% Nb. Due to the small dimension of the phase, the composition may be overestimated. As discussed later, these microstructures indicate that these samples have supercooled against the copper chill.

The microstructures of Al-53 at.% Nb are illustrated in Fig. 6a to d. For samples quenched from a superheating of 200 K, the microstructure contained a primary phase (seen as gray) surrounded by eutectic zones, as illustrated in Fig. 6a. EDS analysis indicated that the primary phase contained 60 to 61 at.% Nb. However, careful etching revealed the presence of two distinct regions within the primary phase: a darker zone, usually associated with higher concentration of Nb (about 61 at.%) located at the circumference, and a brighter central zone, which contained a slightly lower amounts of Nb (close to 60 at.%). The white phase was identified as $AlNb_2$.

The microstructure of samples dropped from the "liquid + solid" state (1873 K), shown in Fig. 6b, was similar to that of samples solidified from the superheated state. The faceted structure, however, was more pronounced, and the composition in the entire cross-section of the primary phase was about 60 at.% Nb. Supercooling the alloy, as shown in Fig. 6c and d, caused the primary $AlNb_2$ phase to become less faceted, and its average Nb concentration to decrease to about 59 and 57 at.% Nb for 195 and 240 K supercooling, respectively.

4. Discussion

4.1. Melting of Al with Nb

The arc melting of Nb-Al alloys was found to produce structures which contained undissolved Nb particles even after several melting processes. This is due to the fact that upon melting of Al in contact with Nb, an

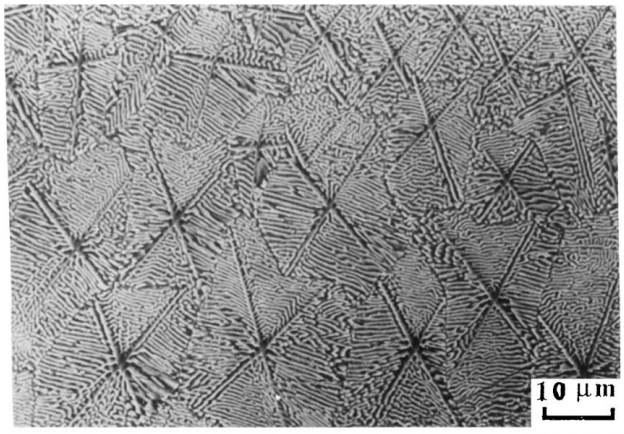

(a)

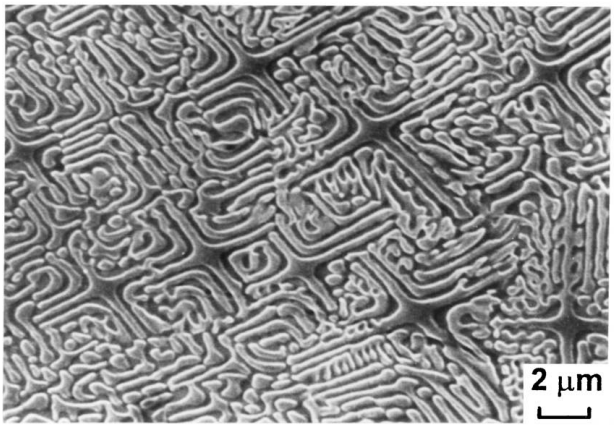

(b)

Figure 5 Secondary electron images illustrating the microstructure of Al 40 at.% Nb dropped from the "liquid" state in regions in specimens which their thickness is less than 0.9 mm at two magnifications.

intermediate layer of Al_3Nb (or in some cases $AlNb_2$) forms initially around the Nb particles. The intermetallic layer prevents further Nb dissolution in the molten aluminum. Increasing the arc melting time does not seem to alleviate the problem since a large portion of the heat input flux is lost through aluminum evaporation, rather than heating and melting of the intermetallic.

In contrast, when EM levitation is used, the heat generation is internal to the sample due to eddy current losses, with the heat generation dependent on the local electrical resistively and susceptibility. Because these for Nb are much larger than those for Al, it is reasonable to assume that initially the Nb pieces are heated to much higher temperatures than the surrounding liquid Al. These factors result in attainment of homogeneous liquid without appreciable vaporization of Al which curb the problems originating during arc melting of Nb and Al samples.

Heating of Al-15 at.% Nb specimens in the levitation apparatus above 933 K, for the first heating cycle initially causes melting of Al while the Nb pieces remain undissolved. However, heating beyond 1773 K causes an accelerated exothermic compound formation between Al and Nb, causing the specimen temperature to rise sharply to about 1890 K. The samples quenched from this temperature were found to be in the "liquid + solid" state. Moreover, quenching of this and other samples showed presence of massive Al_3Nb particles during the ramp temperature rise during the first heating cycle. No Al_3Nb was found in any of the samples with different composition when the temperature was above 1980 K. We thus conclude that the melting temperature of Al_3Nb and the liquidus temperature of Al-15 at.% Nb are 1980 and 1890 K, respectively, as shown on the Al-Nb phase diagram (Fig. 7). These values are about 100 K higher then those reported in the assessed Al-Nb phase diagram reported of 1981 in Bulletin of Alloy Phase Diagram [12], but more closer to the more recent assessed diagram of 1990 [13], and consistent with Kattner's [14] and Beaver *et al.* [15] findings. The latter diagram with the modified boundaries drawn by the dashed-doted line is shown in Fig. 7.

4.2. Effect of supercooling on the microstructure

As discussed below, there are three major effects of supercooling on the microstructure of Al-Nb alloys: microstructural refinement, morphological changes, and extension of solid solubilities.

As was shown in Fig. 3, the Al-15 at.% Nb alloys which solidified during levitation, or dropped on a copper chill from the liquid state without supercooling, had dendritic microstructures whose dimensions depended on the cooling rates or distance from the chill surface or thickness of the quenched splats. When the alloys were supercooled up to 375 K, the dendritic morphology remained the same, but became much finer with the supercooling. For Al-40 at.% Nb, on the other hand, a change in the morphology was also observed as the supercooling was increased. The higher supercooled alloys showed spherical growth domains, as can be seen in Fig. 4e. According to the structural analysis, all the specimens, independent of the solidification conditions, contained only Al_3Nb and $AlNb_2$ phases. The volume fraction of the spherical domains, which contained primary Al_3Nb and $Al_3Nb + AlNb_2$ eutectic, increased with increasing supercooling. The microanalysis showed that the faceted phase contained between 26 and 31 at.% Nb. As will be discussed later and according with the structural analysis, this faceted phase is identified as Al_3Nb with an extended solid solubility of Nb. The phase surrounding the Al_3Nb contained between 48 and 52 at.% Nb, which is identified as $AlNb_2$ with enhanced solid solubility of Al (the structural analysis eliminates the possibility of an AlNb phase which contain 50 at.% Al). However due to the preferred orientation of the solidified samples, and due to the sample dimensions it was hard to determined if there are minor shifts in the XRD peak positions due to the off stoichiometry of the compound. The enhanced solid solubility of Al in the $AlNb_2$ phase was also detected in supercooled Al 53 at.% Nb alloys described below. The $AlNb_2$ phase had faceted appearance at low supercooling, but became non-faceted as supercooling increased.

The microstructure of some Al-40 at.% Nb alloys quenched from the "liquid" state with about 50 K superheating, particularly when the specimen thickness was less than 0.9 mm, exhibited a cellular eutectic

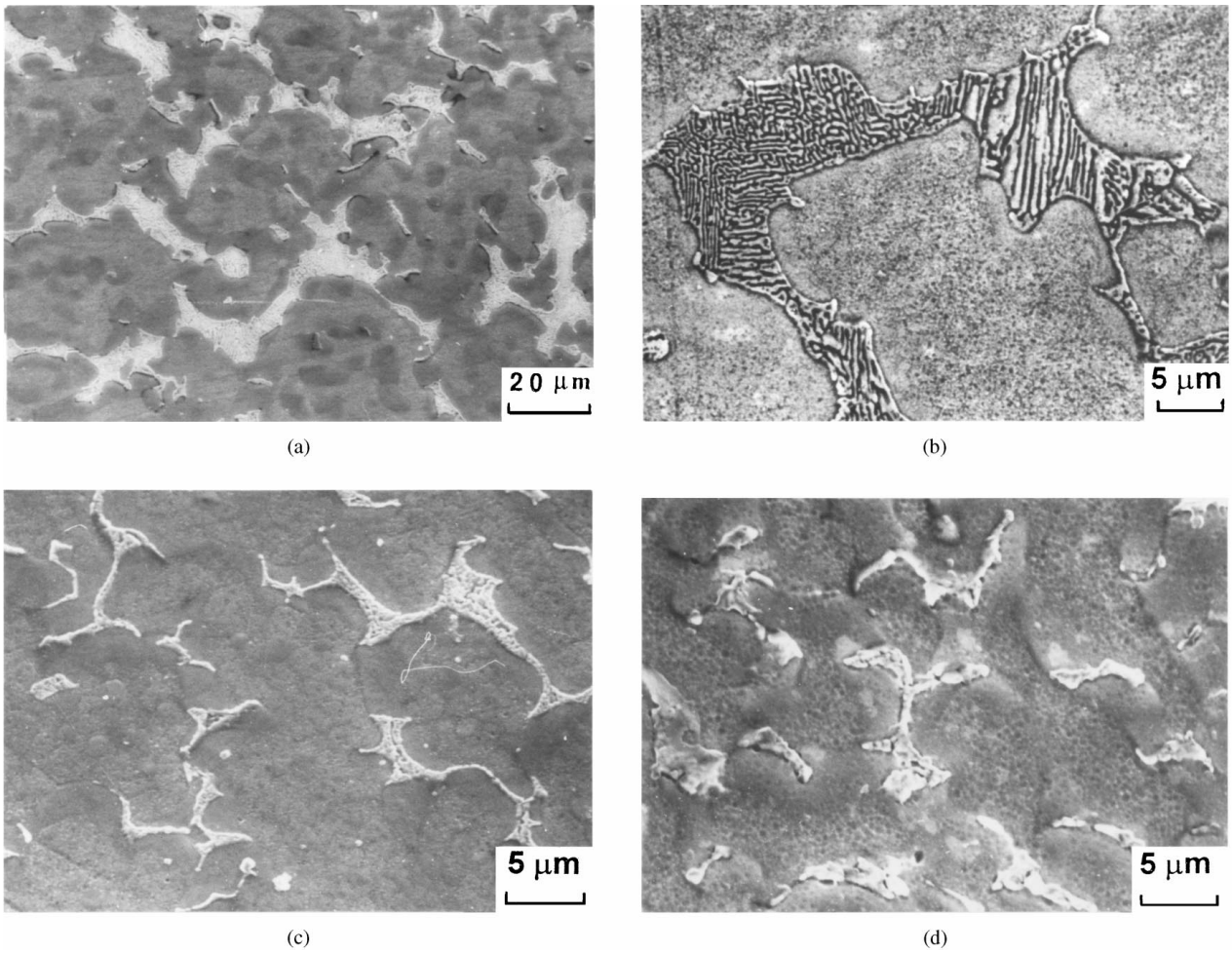

Figure 6 Secondary electron images demonstrating the microstructure of Al 53 at.% Nb specimens solidified under different conditions. a) quenched from 200 K superheat stage, b) quenched from the "liquid + solid" state. c, d) solidified from 75 and 240 K supercooling, respectively.

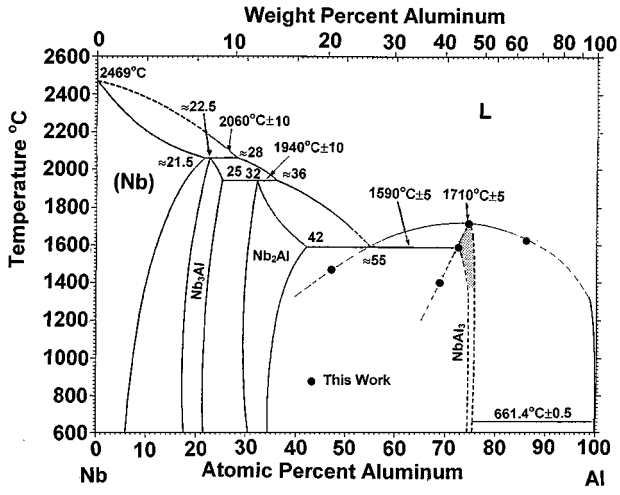

Figure 7 The melting point of Al-15 at.% Nb alloys and of Al_3Nb phase and other compositional EDS analysis are superimposed on the stable Al-Nb phase diagram [12].

microstructure with a dendritic cross in the center of each cell (Fig. 5). X-ray microanalysis indicated that the cross contained up to 28 at.% Nb. These crosses are probably Al_3Nb dendrites of enhanced solid solubility, typical of alloys solidified under bulk supercooling conditions. In a previous work we have found [16] that a dynamic bulk supercooling of about 60 K was obtained in Cu-20 wt.% Co alloys dropped on a copper chill. This was deduced from the fact that the alloys showed clear evidence of solidification in the two-phase miscibility liquid gap. The small sample thickness, the good thermal conductivity of the Cu-Co alloys, and the good heat absorption of the chill were believed to have resulted in a high cooling rates and dynamic bulk supercooling conditions. Moreover, thermal calculations [17] have shown that the amount of supercooling that one may obtain when an aluminum layer of 250 μm thickness is brought into good thermal contact with a massive copper substrate, initially at ambient temperature, is a function of the distance from the copper chill. For example, at a distance of 5 μm one may get as high as 250 K decrease relative to the pouring temperature, while the temperature decrease is only about 130 K at a distance of 50 μm. Therefore, solidification under high cooling rates, such as effected by splat quenching of layers of thickness less than 1 mm on a copper plate, might also involve solidification under bulk supercooling conditions. The appearance of the microstructure in Fig. 5 and the supersaturation of Al_3Nb indicate that these Al-40 at.% Nb samples, although dropped about 50 K superheat, have experienced dynamic bulk supercooling of about 50 K upon contact with the copper chill.

From the microstructures (Fig. 5a and b), it appears that Al_3Nb is the first phase to nucleate with a composition close to 28 at.% Nb, i.e. a metastable

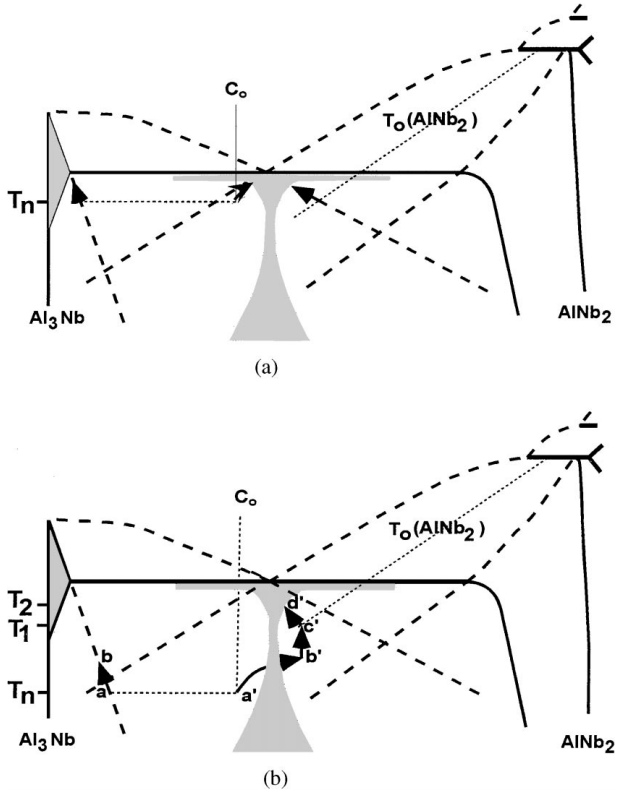

Figure 8 The extended view of the middle part of Al-Nb phase diagram. The metastable extensions of the liquidus and solidus curves of the Al_3Nb and $AlNb_2$ are shown as dashed lines. The suggested solid solubility of Nb in Al_3Nb phase (dashed area) is also superimposed on the phase diagram. a) low supercooling, b) high supercooling.

supersaturation of approximately 3 at.%. The growth of these dendrites causes the composition of the remaining liquid to shift toward the coupled eutectic zone. As shown in Fig. 8a, suppose that nucleation takes at the temperature T_n, which is slightly below the eutectic temperature. At this point, the first phase to solidify is the metastable Al_3Nb. The liberated heat-of-fusion raises the melt temperature and the Nb concentration in the Al_3Nb and the liquid and solid concentrations follow the metastable extensions of the solidus and liquidus lines, respectively, as shown by the solid arrow in Fig. 8a. As solidification proceeds, the remaining liquid enters the coupled-eutectic zone and solidifies with a regular eutectic microstructure.

When the Al-40 at.% Nb liquid was supercooled by more than 60 K before dropping against the chill, spherical growth domains were observed. We suggest that each spherical domain may have resulted from the fragmentation of fine and supersaturated Al_3Nb dendrites, which formed during the early stages after nucleation. For highly supercooled liquids, the rapid formation and growth of the early dendrites is accompanied by a release of the latent heat of fusion, causing not only a local temperature rise but possibly also high local levels of fluid flow. These cause fragmentation of parts of the Al_3Nb dendrites, leaving dendritic elements in the spherical domain. Similar observations were made previously in supercooled Fe-Ni alloys [8]. At low supercooling levels (60 K), the spherical domains contained Al_3Nb fragments, surrounded by the regular eutectic. As supercooling increased, the concentration of the Nb in the Al_3Nb increased up to 31 at.%, and Al_3Nb particles were also surrounded by a phase contained around 48 to 52 at.% Nb. The microstructure observed in the spherical domains can be understood with the aid of the solidification path of Fig. 8b.

When nucleation takes place at large supercooling (T_n of Fig. 8b), first to solidify is again the Al_3Nb phase in the form of dendrites. As solidification proceeds and the temperature increases, the Nb concentration in the Al_3Nb follows the metastable extensions of the solidus (from point (a) to point (b)), as shown by the solid arrow in the figure. At the same time the average liquid composition changes from point (a′) to point (b′). It becomes thermodynamically possible for the $AlNb_2$ phase to nucleate when the liquid composition and temperature shift below T_0 curve (the curve where the solid and the liquid free energies for $AlNb_2$ are equal. We have drawn the T_0 curve midway in the solid-plus-liquid field). The nucleation of $AlNb_2$ can take place at any location below T_0, but most likely at the $NbAl_3$ liquid interface which has the highest Nb build up. The $AlNb_2$ can initially grow partitionlessly (the solid has the same composition as the parent liquid) following the arrow upward (from point b′ to c′). As solidification proceeds, the $AlNb_2$ grows around the Al_3Nb in the solute rich boundary surrounding the latter. At some point, the temperature raises above the T_0 (T_1), and partitioning begins. At the same time the average liquid composition of the melt follows the arrow from point (c′) to (d′), and the remaining liquid enters the coupled eutectic zone (T_2) and the residual melt solidifies as a coupled eutectic growth. It should be noted that the two nucleation events were shown in the thermal response of the levitated sample in Fig. 1b. The first nucleation event took place at point (f), and upon further cooling a second nucleation took place at point (g). While the first phase had slow growth, the second resulted in a massive recalescence. We attribute the first to nucleation of Al_3Nb and the second to $AlNb_2$.

The above solidification path not only explains the sequence of the microstructures, but also the supersaturation of Al_3Nb with respect to Nb and supersaturation of Al_2Nb with respect to Al. It should be noted that the supersaturation for the former phase indicates that Al_3Nb is not a stoichiometric line compound (the dashed area in Fig. 7). The solubility limit in the Nb rich side at the eutectic temperature is estimated as 28 at.% Nb. This findings supports the conclusion that the Al_3Nb has a homogeneity range as reported by the recent assessed phase diagram by Massalski [13], but not with that assessed previously [12].

5. Summary

The microstructure of Al-Nb alloys containing 15 to 53 at.% Nb under different supercooling levels was investigated, yielding the following results:

1) The effects of supercooling as high as 375 K on the microstructure and composition of Al-Nb alloys were investigated.

2) The melting temperature of Al_3Nb and the liquidus temperature of Al-15 at.% Nb are 1980 K and

1890 K, respectively. These values are about 30 K to 100 K larger than the values extracted from known phase diagrams.

3) It was found that Al_3Nb is not a stoichiometric line compound but has a homogeneity Range on the Nb side. The solubility limit at the eutectic temperature could be estimated as 28 at.% Nb.

Acknowledgements

The authors wish to thank Mr. C. Cotler, Mr. Z. Barkai and Mr. G. Engel for their technical assistance.

References

1. J. WADSWORTH, T. G. NIEH and L. J. STEPHENS, *Int. Materials Reviews* **33** (1988) 131.
2. K. R. JAVED and R. ABBASCHIAN, *Materials Science Forum* **50** (1989) 151.
3. R. A. PERKINS, K. T. CHANG and G. H. MEIER, *Scr. Metall.* **22** (1988) 424.
4. R. G. ROWE, A. I. TAUB and F. H. FROES, in "Rapid Solidification Processing, Principles and Technologies IV," edited by R. Mehrabian, and D. Parrishm (Claitorr Publishing, 1986) p. 149.
5. A. MUNITZ and R. ABBASCHIAN, "Undercooled alloy Phases," edited by C. C. Koch and E. W. Collings (The Metallurgical Society of AIME, New Orleans, Louisiana, March 2–6, 1986) p. 23.
6. A. MUNITZ and C. COTLER, "The 4th Israeli Con. Materials Science and Engineering Towards 21st Century," edited by J. Baram, D. Itzhak and D. Eliezer, *Israel J. of Technology* **14** (1988) 133.
7. A. MUNITZ, S. P. ELDER and R. ABBASCHIAN, *Met. Trans. A* **23A** (1992) 1817.
8. G. J. ABBASCHIAN and M. C. FLEMINGS, *ibid.* **14A** (1983) 1147.
9. S. J. REED, "Electron Microprobe Analysis" (Cambridge University Press, Cambridge, 1977) p. 175.
10. A. B. GOKHALE. G. SARKOR, R. ABBASCHIAN, J. C. HAYGORTH, C. WOJCIK and R. E. LEWIS, "Solidification Processing of Eutectic Alloys," edited by D. M. Stefanescu, R. Abbaschian, R. J. Bayuzick (The Metallurgical Society, Inc.) Proceedings of a symposium, October 12–15 1988, Cincinnati, Ohio, 177.
11. L. LU, A. B. GOKHALE and R. ABBASCHIAN, *J. Mat. Sci. & Eng.* (1991).
12. Bulletin of Alloy Phase Diagram, **2** (1981) 75.
13. T. B. MASSALSKI, "Binary Alloy Phase diagrams (2nd ed.) ASM," 1990, p. 179.
14. U. R. KATTNER, Alloy Phase Diagrams Vol. 3, ASM Handbook (The Materials Information Society, 1992).
15. W. W. BEAVER, A. J. STONEHOUSE and R. M. PAINE, "Proc. Metals for the Space Age," Metallwerk Plansee Agm Ruttle/TTTriol, 1965, p. 682.
16. A. MUNITZ and R. ABBASCHIAN, *Met. and Mater. Trans. A.* **27** (1996) 4049.
17. T. W. CLYNE, *Met. Trans. B* **15B** (1983) 369.

Received 15 January
and accepted 11 November 1999